



Dynamic Failure of Materials: A Review

by Cyril Williams and Bryan Love

ARL-TR-5275

August 2010

NOTICES

Disclaimers

The findings in this report are not to be construed as an official Department of the Army position unless so designated by other authorized documents.

Citation of manufacturer's or trade names does not constitute an official endorsement or approval of the use thereof.

Destroy this report when it is no longer needed. Do not return it to the originator.

Army Research Laboratory

Aberdeen Proving Ground, MD 21005-5066

ARL-TR-5275**August 2010**

Dynamic Failure of Materials: A Review

Cyril Williams and Bryan Love
Weapons and Materials Research Directorate, ARL

REPORT DOCUMENTATION PAGE				Form Approved OMB No. 0704-0188	
Public reporting burden for this collection of information is estimated to average 1 hour per response, including the time for reviewing instructions, searching existing data sources, gathering and maintaining the data needed, and completing and reviewing the collection information. Send comments regarding this burden estimate or any other aspect of this collection of information, including suggestions for reducing the burden, to Department of Defense, Washington Headquarters Services, Directorate for Information Operations and Reports (0704-0188), 1215 Jefferson Davis Highway, Suite 1204, Arlington, VA 22202-4302. Respondents should be aware that notwithstanding any other provision of law, no person shall be subject to any penalty for failing to comply with a collection of information if it does not display a currently valid OMB control number. PLEASE DO NOT RETURN YOUR FORM TO THE ABOVE ADDRESS.					
1. REPORT DATE (DD-MM-YYYY) August 2010		2. REPORT TYPE Final		3. DATES COVERED 28 April 2010–1 July 2010	
4. TITLE AND SUBTITLE Dynamic Failure of Materials: A Review				5a. CONTRACT NUMBER	
				5b. GRANT NUMBER	
				5c. PROGRAM ELEMENT NUMBER	
6. AUTHOR(S) Cyril Williams and Bryan Love				5d. PROJECT NUMBER AH80	
				5e. TASK NUMBER	
				5f. WORK UNIT NUMBER	
7. PERFORMING ORGANIZATION NAME(S) AND ADDRESS(ES) U.S. Army Research Laboratory ATTN: RDRL-WMT-D Aberdeen Proving Ground, MD 21005-5066				8. PERFORMING ORGANIZATION REPORT NUMBER ARL-TR-5275	
9. SPONSORING/MONITORING AGENCY NAME(S) AND ADDRESS(ES)				10. SPONSOR/MONITOR'S ACRONYM(S)	
				11. SPONSOR/MONITOR'S REPORT NUMBER(S)	
12. DISTRIBUTION/AVAILABILITY STATEMENT Approved for public release; distribution is unlimited.					
13. SUPPLEMENTARY NOTES					
14. ABSTRACT This report reviews the dynamic failure of materials. Compared to static or quasi-static failure, dynamic failure deals with the fracture process for which the effects of inertia cannot be ignored. Dynamic failure, when compared to the well-established classical fracture mechanics, is considered to be a relatively new field of study. For clarity, this report is divided into several sections. The first section is a brief historical background on the dynamic failure process, followed by a concise description of ductile fracture of homogeneous materials from the spallation and fragmentation point of view. The brittle fracture process is then briefly described from the dynamic failure point of view. Lastly, both numerical and experimental techniques used for studying dynamic failure are described. This report is not an exhaustive review on the topic of dynamic fracture but provides enough relevant information for the basic understanding of the dynamic fracture process.					
15. SUBJECT TERMS dynamic, failure, ductile, fracture, brittle, spall, experiment, modeling					
16. SECURITY CLASSIFICATION OF:			17. LIMITATION OF ABSTRACT UU	18. NUMBER OF PAGES 42	19a. NAME OF RESPONSIBLE PERSON Cyril Williams
a. REPORT Unclassified	b. ABSTRACT Unclassified	c. THIS PAGE Unclassified			19b. TELEPHONE NUMBER (Include area code) 410-278-8753

Contents

List of Figures	iv
1. Introduction	1
2. Ductile Fracture of Homogeneous Materials	3
2.1 Spallation and Fragmentation: Void Nucleation and Growth	4
3. Brittle Fracture	12
4. Numerical Methods in Dynamic Failure	14
5. Experimental Techniques	17
5.1 Plate Impact	17
5.2 Dynamic Fracture	20
6. Concluding Remarks	24
7. References	25
Distribution List	32

List of Figures

Figure 1. A classic cup-and-cone failure surface resulting from a ductile fracture under quasi-static load conditions.....	3
Figure 2. Plate impact flyer-target experimental setup.....	4
Figure 3. A simplified distance-time (Lagrangian) plot showing the propagation of waves in the flyer and target after impact.....	5
Figure 4. Dynamic deformation system (23).....	6
Figure 5. A region of rapidly expanding fluid that will eventually result in a fragment (25).	7
Figure 6. Kinetic energy vs. surface area with the minimum as the fracture area (25).	7
Figure 7. Comparison between calculated and experimental data for oil shale (25).	9
Figure 8. Spherical void in a remote simple tension strain rate field (39).....	11
Figure 9. Dynamic aspects associated with mechanical testing (76).....	17
Figure 10. (a) Lagrangian or time-distance diagram and (b) the velocity-time history of a two-structure wave.....	18
Figure 11. A schematic representation of the VISAR system.	20
Figure 12. Method of caustics applied to edge-impacted pre-cracked PMMA specimen, resulting in mode-II dominant cracks (87).....	22
Figure 13. Diagram of coherent gradient sensing experimental setup for reflective materials (from Rosakis et al. [91]).	23

1. Introduction

Dynamic fracture mechanics is a specialized branch of engineering that deals with the fracture phenomena for which the role of material inertia cannot be ignored. Dynamic fracture is a subfield of fracture mechanics. In general, the effects of inertia cannot be ignored when loads are applied at relatively high rates to a solid body with an existing crack or from a rapidly growing crack. Normally, when such bodies are subjected to surface tractions, the crack may or may not propagate, depending on the magnitude and rate at which the traction is applied. For low rates, classical fracture mechanics may be used to solve the problem in which fracture can be predicted once the stress level reaches a critical value. However, for high rates, the crack may propagate instantaneously, depending on the magnitude of the stress wave and the rate at which it is applied. Therefore, the stress field around the crack tip is not in equilibrium, and the inertial effects cannot be ignored.

Unlike classical fracture mechanics which is somewhat well established, dynamic fracture mechanics is relatively new when compared to other branches of engineering. Although some advances have been made over the past few decades, the laws governing the behavior of cracks when subjected to stress waves are still in their infancy; therefore, the approach to analyzing such problems is based on qualitative reasoning and experience with known solutions to specific problems (*1*).

A popular concept in the treatment of fracture initiation and propagation due to dynamic loading is the stress intensity concept. It provides a basis for quantifying the resistance of materials to the onset of growth of an existing crack. The basis for this approach can be traced back to the Irwin criterion in classical fracture mechanics. This criterion states that the onset of crack growth occurs when the stress intensity factor of a material has risen to a critical value called the fracture toughness, K_{IC} . The experimental determination of K_{IC} can be quite difficult. Similarly, dynamic fracture experiments are extremely difficult and expensive to execute because the equipments involved require a steep learning curve and high cost. For this reason, fewer than 100 facilities around the world pursue dynamic fracture experiments.

During the 19th century, limited forms of high strain rate experimentations were performed on military ordnances and industrial machines. However, no major breakthrough can be identified as the launching pad for dynamic fracture mechanics as an area of research until the early 1970s when the importance of understanding crack propagation and arrest was recognized in both engineering and earth sciences. Some of the ideas developed for fracture under equilibrium conditions are also useful for dynamic fracture. The work by A. A. Griffith (*2*) is considered to be one of the earliest in equilibrium fracture mechanics that is useful as a quantitative science in material behavior. Plane elasticity solution for a crack of finite length in a body subjected to a

uniform remote tension in a direction normal to the crack plane was the basis of Griffith's original work. Griffith, when considering an ideally brittle elastic body containing a crack, recognized that the macroscopic potential energy of the system, which consists of the internal stored elastic energy and the external potential energy of the applied loads, changes as the crack grows. Furthermore, Griffith realized that due to the growth of the crack or crack extension, new crack surfaces are created. Therefore, he postulated that a certain amount of work per unit area of crack surface must be expended at a microscopic level to create that surface. This work per unit area is usually characterized by assuming that a particular force-displacement relationship controls the reversible interaction of atom or molecules across the fracture plane. Griffith's energy condition is of particular interest to engineers and scientists because it renders the need to examine in detail the actual fracture process at the crack tip unnecessary.

There were several important works relating to fracture worth mentioning after that of A. A. Griffith. Sir Neville Mott (3) proposed a theoretical framework that includes inertial effects during the rapid crack growth phase. At high crack speeds, Mott realized that inertial resistance of the material to crack opening could become significant. Mott assumed that the crack growth process was time independent in order to estimate the crack speed for a specific loading system. However, it was later shown that Mott's assumptions of the dynamic Griffith crack were not valid, and therefore the resulting conclusions were also not valid. George Irwin (4), concerned with cleavage fracture of structural steels, developed another important theoretical idea for applying work and energy methods to fracture dynamics. Although Irwin adopted Mott's postulate of total energy, which includes a work of fracture, he proposed that the work of fracture may be approximately represented as the sum of two proportional terms. These are the area of fracture surface and the volume of material affected by plastic deformation. This idea therefore expanded the applicable range of the energy balance fracture theory to materials that undergo some plastic deformation during crack extension. Later in 1957, Irwin (5) introduced the concept of elastic stress intensity factor and proposed that the onset of crack growth in a cracked body with limited plastic deformation at the crack tip is when the elastic stress intensity factor (K_I) reaches a critical value called the fracture toughness. Under plane strain conditions, the stress intensity factor can be related to the energy release rate (G) by the equation

$$G = \frac{(1-\nu^2)}{E} K_I^2, \quad (1)$$

where ν is the Poisson's ratio and E is the elastic or Young's modulus. There are numerous important studies on dynamic fracture of materials that were executed concurrently with the concepts for analyzing cracked solids subjected to dynamic loads. For more information on experimental dynamic fracture research of engineering materials, the reader is encouraged to review refs 6–15.

2. Ductile Fracture of Homogeneous Materials

In general, the term “ductile fracture” implies that during a failure or fracture process, the fractured material suffered large amounts of plastic deformation. This is somewhat misleading since cleavage or brittle failure sometimes occurs after considerable plastic deformation in some materials. Usually under quasi-static loading conditions, ductile fracture is characterized by a cup-and-cone failure surface, as shown in figure 1. This classic form of failure is a result from a complex process arising from the stress distribution in a uniaxial tensile test and also the work-hardening characteristics of the material being tested. There are other types of failure surfaces resulting from ductile fracture, such as the double cup and cone, which is usually observed in ductile materials with an average work hardening and a low inclusion density. Another failure surface type is a planar surface that is associated with high strength materials with high inclusion content and a low work-hardening rate.

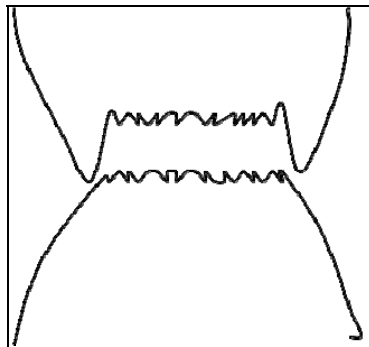


Figure 1. A classic cup-and-cone failure surface resulting from a ductile fracture under quasi-static load conditions.

How these macroscopic failure surfaces formed is dependent on the microscopic fracture mechanisms and the development of the neck. Usually, a neck can occur when the increase in tensile stress due to the reduction in cross-sectional area as a result of plastic deformation can no longer be supported by the concurrent strain hardening. A triaxial state of stress can exist in the necked region after a neck is formed due to the nonuniformity of the necked region. This triaxial stress state is extremely important when controlling the fracture characteristics of a material. Metallographic studies performed on the necked region of deformed materials have shown that during the early stages of necking, slip is the dominating factor. However for large deformations, voids are nucleated, then grow, and coalesce to form cracks. These cracks ultimately cause material failure. The nucleation, growth, and coalescence of these voids are extremely susceptible to stress triaxiality.

2.1 Spallation and Fragmentation: Void Nucleation and Growth

The basic definition of spall fracture is when two plane decompression waves subjected to uniaxial strain conditions collide to produce a region of tension in the interior of a material body sufficient to cause fracture. Plate impact experiments are typically used for studying spall fracture. As shown in figure 2, the plate impact specimen test setup mainly consists of a flyer and a target plate. The flyer plate is normally launched using either a gun system with the aid of a sabot or an explosive toward a stationary target plate. Upon impact, two compression waves are generated at the flyer-target interface, as shown in figure 3, and they travel in opposite directions. Once they get to the free surface of both the flyer and target, they are reflected as decompression waves (or rarefaction waves). Upon collision of the two decompression waves, a region of high tension is produced. Strain rates of 10^4 to 10^6 s^{-1} are typical for plate impact tests, and the resulting stress can be extremely high when compared to the quasi-static strength of even the strongest materials. Therefore, the material fails by spallation. It is worthy to note that the back face or free surface velocity of the target is monitored using a Velocity Interferometer System for Any Reflector (VISAR). The pull back velocity obtained from the velocity profile of the back face velocity is used for estimating the spall strength of the material in question.

Hopkinson (16) was credited with the earliest observation of spall fracture, and later in the early 1960s, it was subsequently studied in some depth by Kolsky (13) and then Rinehart and Pearson (17). During the 1960s, research on spall fracture became more intense and more quantitative as approaches were taken which led to theories that took into account the complexity of material behavior. The bulk of this research was conducted by three groups: the Stanford Research Institute (SRI), Los Alamos National Laboratory, and Sandia National Laboratory (SNL). The majority of this section will focus on the early work at SNL and SRI. Starting around the mid 1970s, D. P. Dandekar and his colleagues at U.S. Army research establishments all around the United States were developing novel spall testing techniques and studying the response of different materials, especially ceramics, to support novel armor designs. Their research as it relates to ballistics is reserved for further review by the authors.

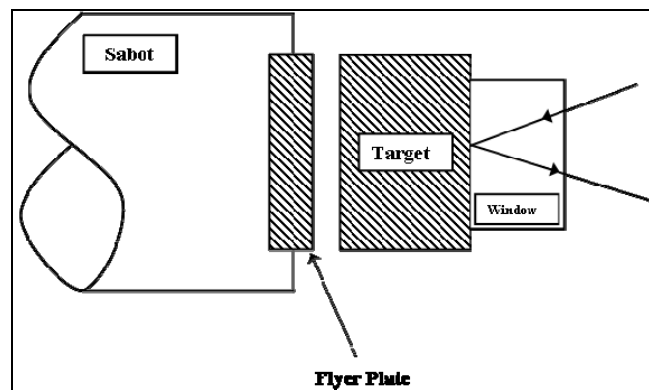


Figure 2. Plate impact flyer-target experimental setup.

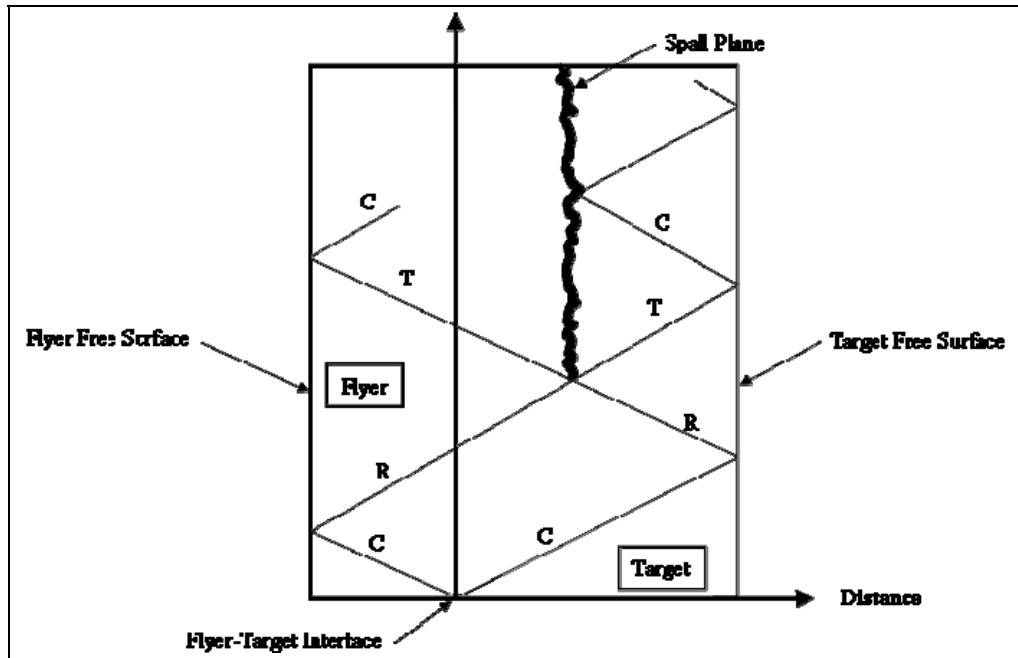


Figure 3. A simplified distance-time (Lagrangian) plot showing the propagation of waves in the flyer and target after impact.

The effects of the amplitude of the shock compression wave that precede the tensile rarefaction wave were investigated by Stevens and Tuler (18) using plate impact experiments. They concluded that there is no significant effect of varying amounts on the dynamic precompression on the spall strength of 1020 steel and 6061-T6 aluminum. This simply means that shock wave strengthening does not have a significant effect on the spall strength of 1020 steel and 6061-T6 aluminum. However, previous experiments done by Buchanan and James (19) showed that the spall strength of mild steel increased linearly with the precompression amplitude for a pulse duration that was not constant. Stevens and Tuler (18), on the contrary, took into account this notion and kept the pulse duration constant.

After reviewing the current spall criteria at the time and systemizing them, Davison and Stevens (20) introduced the concept of a continuum measure of spalling. They classified the spall criteria into classes, “instantaneous and cumulative” and “local and non-local.” If the spall criteria are dependent only on the current values of the field variables, then the class is “instantaneous” and “cumulative” if the spall criteria are dependent on the history of the field variables. Furthermore, if the values of field variables at the spall plane are used in the determination of damage, then the class is local and non-local if the field variables at distant locations have a role on the determination of damage. The theory proposed by Davison and Stevens (20) was phenomenological in that no detailed mechanisms for the initiation and propagation of micro-failures were included. However, in 1973, Davison and Stevens (21) proposed a more detailed

theory for spall related damage in which failure occurs by the initiation and propagation of cracks. This was applicable to alloys exhibiting brittle behavior subjected to dynamic loads. In 1977, a comprehensive report was published by Davison et al. (22) on the theory of ductile spall damage where spalling occurs by void nucleation, growth, and coalescence. Figure 4 is a schematic representation of ductile and brittle spall fracture resulting from a projectile impacting a target.

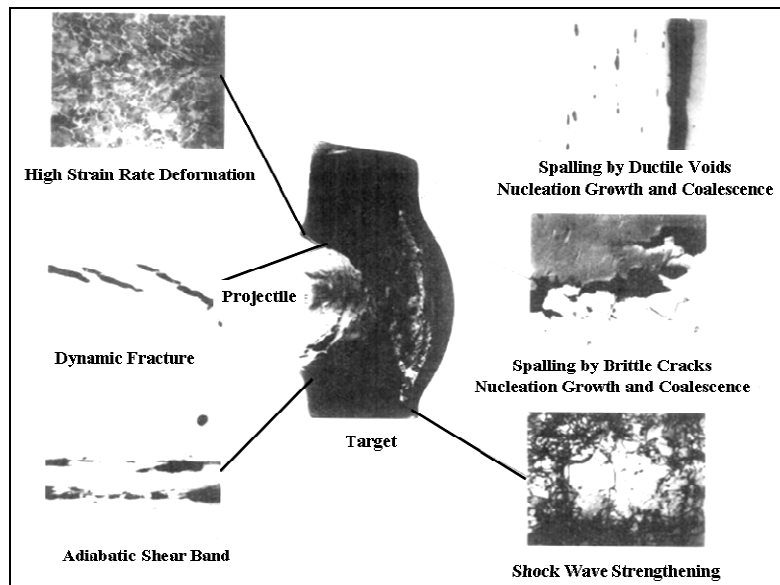


Figure 4. Dynamic deformation system (23).

Over the past two decades, several theories and experimental methods have been developed for predicting the behavior and, consequently, the fragmentation resulting from explosively driven cylinders or high-velocity impacts. Mott's theory (24) on the expansion of an explosively driven ring and its resulting fragmentation was expanded by Grady (25). Grady calculated the fragment size distribution for the case of ductile fracture using survival statistics, and the results compared favorably with the experimental results obtained by Wesenberg and Sagartz (26) for an expanding 6061-T6 aluminum cylinder. A general expression for the sizes of fragments was cleverly developed by Grady based on an energy balance approach. The basic principles of the energy balance approach are that the interfacial energy generated by the fragmentation process is balanced by the local inertial or kinetic energy of the material. This approach was first applied to the dynamic fragmentation in a fluid, as shown in figure 5, and was then extended to brittle materials by incorporating the appropriate fracture mechanics concepts. The instantaneous thermodynamic and kinematic state is provided by the density ρ , density rate $\dot{\rho}$, and temperature θ , which may, in general, be functions of position. Surface tension alone resists the fracturing process. It is intuitive that after complete fracture, the fragments will move away with a specific velocity and hence kinetic energy. Because the fragments continue to fly away, the kinetic

energy of the center of mass of each fragment is maintained, and the fragments do not contribute to the generation of new surfaces. The energy terms are plotted as a function of fracture area in figure 6, and the fragment size is determined by the $dE/dA = 0$, which is the minimum of the curve.

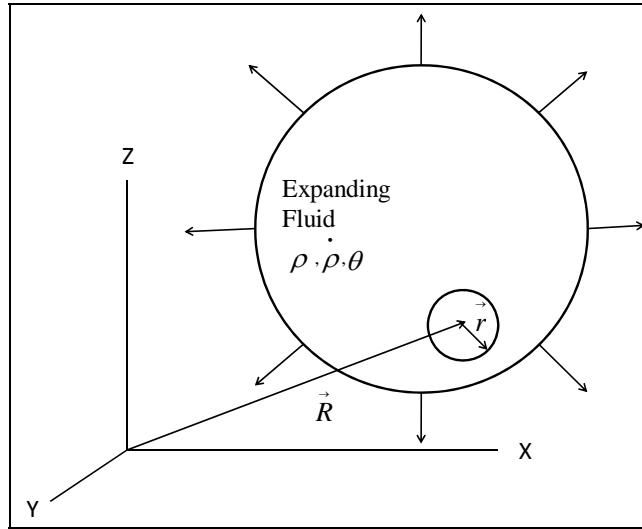


Figure 5. A region of rapidly expanding fluid that will eventually result in a fragment (25).

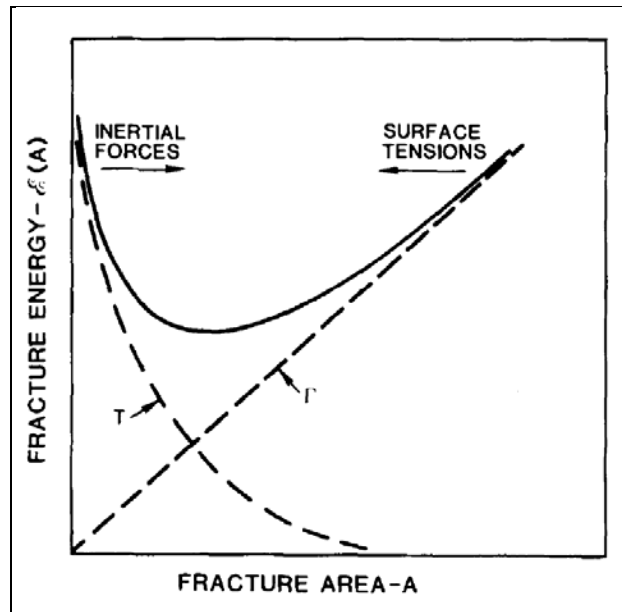


Figure 6. Kinetic energy vs. surface area with the minimum as the fracture area (25).

At equilibrium ($dE/dA = 0$), the fragment surface area to volumetric ratio is

$$A = \left(\frac{3\dot{\rho}^2}{5\rho\gamma} \right)^{1/3}, \quad (2)$$

where γ is the surface energy per unit area. If the fragments are assumed to be spherical and of equal sizes, then the fragment diameter, d , is

$$d = \frac{6}{A}. \quad (3)$$

Therefore,

$$d = 6 \left(\frac{5\rho\gamma}{3\dot{\rho}^2} \right)^{1/3}. \quad (4)$$

The elastic stored energy has to be considered for solids; therefore, the equation connecting fracture mechanics to the surface tensions is

$$\gamma = \frac{K_{IC}^2}{2\rho C^2}, \quad (5)$$

for which K_{IC} is the fracture toughness, C is the sound speed, and ρ is the density of the material.

If equations 2, 3, and 5 are used along with $\dot{\epsilon} = \frac{\dot{\rho}}{3\rho}$ the following expression for the fragment diameter can be derived:

$$d = \left[\frac{(20)^{1/2} K_{IC}}{\rho C \dot{\epsilon}} \right]^{2/3}. \quad (6)$$

Figure 7 shows the relationship between fragment size and strain rate for oil shale. There is good agreement between the experimental and calculated data.

Grady's (25) approach could be generalized by including the crack-tip plasticity into the calculations as explained by Hertzberg (27). The effective crack length is computed by including some fraction of the plastic deformation zone ahead of the crack, and for plane strain, the plastic zone radius, r_y is estimated to be

$$r_y = \frac{1}{6\pi} \left(\frac{K}{\sigma_{ys}} \right)^2, \quad (7)$$

where K is the stress intensity factor and σ_{ys} is the yield stress. Furthermore, the effective stress intensity factor can be deduced by increasing the crack length ' a ' by r_y and therefore

$$K_{eff} = \sigma [\pi(a + r_y)]^{1/2}. \quad (8)$$

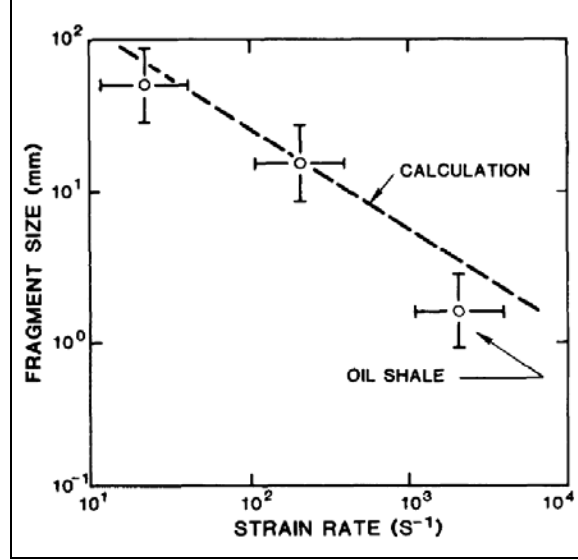


Figure 7. Comparison between calculated and experimental data for oil shale (25).

By substituting equation 7 into 8, the effective stress intensity factor (K_{eff}) can be determined in terms of the stress intensity factor (K). Because the onset of plasticity is determined when the stress (σ) is equal to the yield stress (σ_{ys}), the effective stress intensity factor (K_{eff}) can be determined to be $1.41K_{IC}$. This implies that equation 6 can be written as

$$d = \left[\frac{(20)^{1/2} K_{eff}}{\rho C \dot{\epsilon}} \right]^{2/3} = \left[\frac{6.3 K_{IC}}{\rho C \dot{\epsilon}} \right]^{2/3}, \quad (9)$$

which is the diameter of the fragment in terms of fracture toughness, density, sound speed, and strain rate.

In the early 1970s, the SRI played a vital role in explaining the spall failure process in terms of void nucleation, growth, and coalescence. They systematically measured cracks, void sizes, and their orientation at different stages of the spall process and used their result to develop the Nucleation and Growth (NAG) model. They developed metallographic techniques that are extremely important for quantifying parameters describing the damage accumulation process. By systematically collecting and processing data for a number of materials, Curran et al. (28–36) laid the ground work for the fundamental understanding of the rate of nucleation and the rate of growth of micro-cracks and voids. They developed the equations that described the rate of nucleation \dot{N} and the rate of growth \dot{R} (dR/dt) to be

$$\dot{N} = \dot{N}_0 \exp[(\sigma - \sigma_{no})\sigma_1] \quad (10)$$

and

$$\dot{R} = \left(\frac{\sigma - \sigma_{go}}{4\eta} \right) R, \quad (11)$$

where \dot{N}_0 is the threshold nucleation rate, σ_{no} is the tensile threshold stress, σ_1 is the stress sensitivity for nucleation, σ_{go} is the threshold stress for growth, and η is the viscosity of the medium. It is worth noting that the limiting growth rate for cracks is the Rayleigh wave speed. From equation 10, it is clear that below σ_{no} , the tensile threshold stress, no new voids are nucleated, but if σ_{no} is surpassed, the nucleation rate increases exponentially with the tensile stress σ . Equation 11 reveals that the growth rate \dot{R} is proportional to the radius of the void or crack. As the Rayleigh wave is approached, this proportionality breaks down for a crack. It has been shown that for spherical voids the relative void volume is given by

$$V_v = \frac{8\pi\dot{N}R_0^3}{3[(\sigma - \sigma_{go})/4\mu]} \left[\exp\left(\frac{3(\sigma - \sigma_{go}) \cdot t}{4\mu}\right) - 1 \right], \quad (12)$$

where R_0 is the smallest possible void radius. This was assumed to be 1 μm by Barbee et al. (29). A one- or two-dimensional (2-D) Lagrangian or Eulerian code can be developed to predict relative void volumes and void concentrations as a function of distance from the back face of the target specimen once the parameters of equations 10, 11, and 12 are determined. The NAG-FRAG code was developed by SRI using the approach just described.

Interestingly, the mechanisms for ductile failure in both quasi-static and dynamic load conditions are nucleation, growth, and coalescence of micro-voids. The growth of voids when subjected to quasi-static loads has been treated theoretically by McClintock (37, 38), Rice and Tracey (39), and Needleman (40). McClintock analyzed cylindrical voids subjected to a plane strain condition and concluded that the expansion of the cylindrical voids eventually leads to their coalescence. His analysis also shows a very strong inverse dependence of fracture strain on the tensile stress transverse to the voids. This is quite important to the spall process, where the uniaxial strain condition creates strong transverse tensile stresses in the spall zone. And as expected, very little plastic deformation is actually observed, hence the resulting fracture strain during spallation is invariably low. Needleman studied the interaction between the stress fields of voids. In his analysis, double periodic arrays of parallel cylindrical voids were considered. Using a variational method, he estimated the changes in void shape and size with increasing overall strain and was also able to track the development of the plastic zone around the void.

Using a first approximation of the variational principle, Rice and Tracey (39) analyzed a spherical void of radius R_0 , as shown in figure 8. They assumed that the remote strain field consists of a tensile stretch at the rate $\dot{\epsilon}$ with respect to the x_3 direction and contractions at a rate of $\frac{1}{2}\dot{\epsilon}$ in both the x_1 and x_2 directions (this is a requirement for plastic incompressibility). Rice and Tracey found the velocity field to be in the form

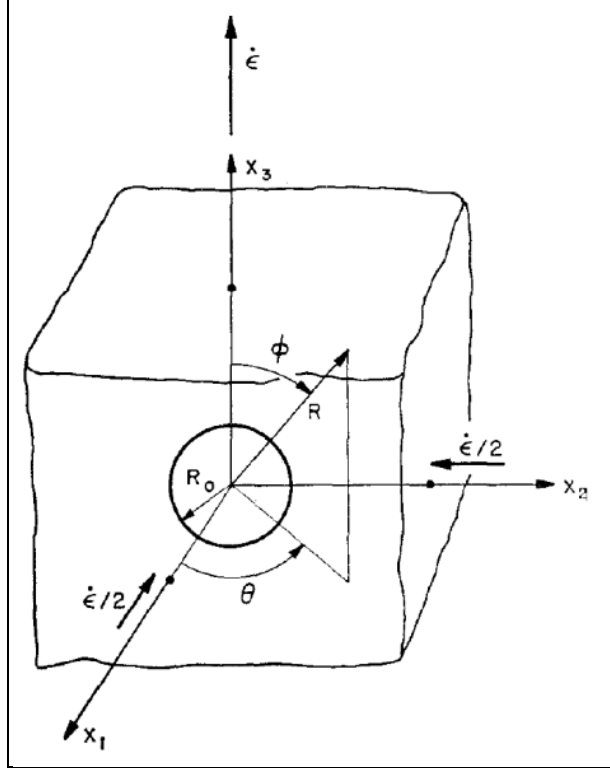


Figure 8. Spherical void in a remote simple tension strain rate field (39).

$$\dot{u}_i = \dot{\epsilon}_{ij}^{\infty} x_j + D\dot{u}_i^D + E\dot{u}_i^E, \quad (13)$$

where D and E are constants, \dot{u}_i^D is a spherically symmetric volume changing field, and \dot{u}_i^E is a shape-changing field that preserves void volume. Because of incompressibility and spherical symmetry, the volume-changing field is required to be

$$\dot{u}_i^D = \dot{\epsilon} \left(\frac{R_0}{R} \right)^3 x_i. \quad (14)$$

Furthermore, Rice and Tracey (39) considered void growth in a general remote strain rate field with high stress triaxiality and found the velocity field to be

$$\dot{u}_i = \dot{\epsilon}_{ij}^{\infty} x_j + D\dot{u}_i^D, \quad (15)$$

where

$$\dot{u}_i^D = \left(\frac{2}{3} \dot{\epsilon}_{ij}^{\infty} \dot{\epsilon}_{ij}^{\infty} \right)^{1/2} \left(\frac{R_0}{R} \right)^3 x_i. \quad (16)$$

Rice and Tracey (39) concluded that the growth rates for spherical voids are significantly elevated by the superposition of hydrostatic tension on a remotely uniform plastic deformation field. For moderate to high stress triaxiality, the relative void growth rates are amplified over imposed strain rates by a factor depending exponentially on the mean normal stress.

3. Brittle Fracture

As opposed to spallation/void nucleation and coalescence, the fracture of materials typically focuses on the propagation of an existing crack or discontinuity. The highly researched field of fracture mechanics spans a wide range of rates (to include fatigue, quasi-static, and dynamic fracture), types (from the brittle linear elastic fracture mechanics to the evolution of shear cracks in the wake of shear localizations), and materials (including glasses, polymers, metals, adhesives, and more). In this section, we focus on high strain-rate brittle fracture of materials.

Linear Elastic Fracture Mechanics (LEFM) is the classic example of brittle material failure. Griffith's (2) theory of fracture, extended to elastodynamics, revealed some interesting results. Yoffe (41) considered a crack of constant length traveling in an elastic medium at a fixed speed; her work indicated that an instability in the problem existed as the speed of the crack approached the Rayleigh (surface) wave speed (C_R). Baker (42) extended this problem to a transient analysis and demonstrated a similar prediction of bifurcation of the crack when its velocity approached the Rayleigh wave speed. Freund (43) offers a comprehensive review of the work in elastodynamics in his monograph, to include the analytical solutions for modes I, II, and III cracks. The idea of a "limiting velocity" sparked many experiments and assessments of crack velocities with respect to loading, some of which will be discussed subsequently.

Schardin (6) and his coworkers utilized a multiple-spark camera in an attempt to observe crack propagation at increasing crack velocities in various types of glass. They confirmed the existence of a limiting velocity for crack propagation and showed that at higher driving forces, the crack bifurcates into two or more cracks rather than increasing in speed. However, the limiting velocity that Schardin observed was substantially lower than the Rayleigh wave speed in some materials it was as low as 30% C_R . Furthermore, this limiting velocity was material dependent, and Schardin proposed that this was an additional material property rather than an independent mechanical mechanism. Kerkhof (9) utilized a separate experimental technique where an ultrasonic transducer input a small amplitude stress wave during the fracture event, resulting in ripples on the fracture surface whose frequency can be correlated to the crack velocity. Kerkhof's technique confirmed Schardin's findings, and by examining a wider variety of glasses, he found that the composition of the glass significantly affected the limiting crack velocity.

The reduced (less than the Rayleigh wave speed) limiting velocity has been the subject of much discussion. Ravi-Chandar and Knauss (44–47) conducted an extensive study of dynamic fracture in a brittle polyester-based polymer (Homalite 100), noting that the surface finish of the fracture surfaces shows distinct regimes during crack propagation. The transition from “mirror” to “mist” to “hackle” showed that the crack demonstrated an increasing tendency toward branching/unsteady propagation as the crack velocity increased. The authors proposed that effects at the micro-scale played a significant role in the macro-scale crack propagation. The formation of micro-cracks ahead of the macro-crack tip led to “discontinuous” or start/stop crack motion as the crack jumped between micro-cracks, and these micro-cracks began to form in more substantial numbers as the crack velocity increased, which resulted in bifurcation at some critical point. The formation of these micro-cracks is inconsistent with the linear elastic theory, explaining the (1) significantly lower limiting velocity than predicted by traditional theory and (2) difficulty in measuring a dynamic fracture toughness (K_D) that predicts the behavior of this type of material. In contrast, most metals undergo yielding near the crack tip without the formation of the micro-cracks. The linear elastic theory can be modified to account for some localized plasticity (e.g., see Freund [43]), and the resulting theory can be used to predict a dynamic fracture toughness. Experimental efforts have shown that it is possible to measure the dynamic fracture toughness of a metal as a function of crack speed (e.g., Pandolfi, et al. [48]), and that theoretical/numerical models can replicate experimental results.

The dynamic propagation of mixed-mode cracks has also been of great interest, especially given the impact/penetration scenario as a driving impetus. Kalthoff and Winkler (49) introduced the loading cracks by edge impact (LECEI) technique to examine cracks propagating in metals for shear (mode II) and mixed mode (mode I/II) conditions. Using the method of caustics, Kalthoff and Winkler observed that failure modes can transition from a principal stress (tensile) crack to a primarily shear (mode II) crack by increasing the driving force significantly, implying that mode II cracks are significantly higher energy than pure mode I cracks in the same material. Furthermore, for some materials the shear crack was ductile in nature, primarily resulting from the formation of a shear localization (adiabatic shear band) and the resulting void nucleation and coalescence. Other researchers (e.g., Zhou et al. [50]) have observed similar behavior, including the formation and propagation of shear bands, in metallic materials. Pure mode II cracks have exhibited some interesting behavior for specific systems. Rosakis et al. (51) observed mode II cracks propagating along weak planes in a brittle polyester resin at speeds in excess of the shear wave speed of the bulk material, resulting in shear shock waves. This phenomenon (detailed in Rosakis [52]), particularly of interest to seismologists and earthquake engineers, allows cracks to propagate at extremely high speeds in high-energy events where other crack modes are prohibited by confinement.

Dynamic brittle fracture has a rich history and a tremendous amount of past research—it would be impossible to reference every researcher here. Freund’s (43) monograph and the book by Ravi-Chandar (53) give a more comprehensive theoretical discussion of dynamic fracture research.

4. Numerical Methods in Dynamic Failure

Accurate simulation of the dynamic failure of materials has been an elusive goal in the material modeling and numerical methods communities for over 20 years. Both communities have a similar problem—dynamic failure is an inherently local, discontinuous change in the behavior of the material through the creation of new surfaces. For material modelers, the local nature of the failure makes it difficult to observe in the laboratory, and the length and timescales of dynamic failure frequently require consideration of material microstructure and defects. The discontinuity produced by failure complicates many traditional numerical methods (such as standard finite element formulations), which rely on continuous state variables over a finite discretization for their solutions. Each community has developed several interesting methods to approach dynamic failure.

Computational methods for simulating dynamic failure can usually be categorized as either continuum or discrete methodologies. Continuum methods are typically implemented much like constitutive models in that material “failure” (such as loss of deviatoric or total strength) is denoted at an integration point of a finite element (or other numerical method). Discrete methods make an attempt to denote the formation of new surfaces, either through mesh/particle re-mapping or through the introduction of additional kinematics that accounts for the formation of the surfaces. Each method has its benefits and limitations, sometimes frequently controlled by implementation as much as physical accuracy.

Continuum damage mechanics (CDM) focuses on the introduction of a “damage” variable that describes the degradation of strength and/or modulus. Introduced in 1958 by L. M. Kachanov (54), CDM has spawned a tremendous number of material/failure models ranging from plasticity to brittle failure to porosity evolution. CDM assumes that the irreversible processes occurring on length scales below the one of interest can be captured using a set of state variables whose evolution is controlled by thermomechanical phenomena measurable on the current length scale. Ductile failure models such as the Johnson-Cook failure (55), Gurson (56), and TEPLA (57, 58) models are designed with CDM in mind; the length scale of void nucleation and growth is such that explicit representation is difficult to capture with realistic computational times. Ballistic impact on brittle materials results in the evolution of innumerable micro-cracks; in an attempt to

model this behavior, numerous researchers (e.g., Rajendran and Grove [59], and Johnson and Holmquist [60]) have used CDM methodologies to denote the loss of strength as the micro-crack density increases.

CDM is also used extensively in the composite materials community because of the multiple failure modes present in a heterogeneous material with a small internal length scale. Most “multi-scale” methods utilize a form of CDM to transfer information from the meso-scale to the macro-scale; for example, the multi-continuum theory for composite materials proposed by Mayes and Hansen (61) transfers damage from the fiber and matrix constituents to the macro-scale through a set of internal state variables. One principal advantage of CDM is that it accommodates progressive damage—certain failure modes/types demonstrate a non-catastrophic loss in material strength (such as porosity evolution), which is difficult to capture with discrete methods without resorting to simulating individual voids. CDM is also straightforward to implement—in many cases, it’s simply adding an additional subroutine to existing material models. However, CDM’s implementation at integration points also leads to a high degree of mesh sensitivity and/or mesh texturing for localized failures (such as brittle cracking). Furthermore, as the stiffness of the element/particle/integration unit is reduced to nearly zero, distortions can become unacceptably large, and a secondary method of damage (element deletion, void insertion, etc.) is needed.

Cohesive zone methods have gained popularity over the past 15 years because of their straightforward application to finite element analyses. Cohesive theories of fracture, such as those proposed by Dugdale (62) and Barenblatt (63), offer a different theory of what is happening in the process zone near a crack tip. These theories assume that in a small region ahead of the crack tip, the area of adhesion decreases progressively, thus resulting in a lowered traction along the “new” crack surface. The traction vanishes at a specified opening displacement, resulting in an irreversible energy loss, which is taken to represent the Griffith energy. The idea of a process zone and the removal of the singularity present in linear elastic fracture mechanics (and thus the incorporation of an inherent length scale) make cohesive zone theory ideally suited for discretized methods.

Xu and Needleman (64) demonstrated cohesive zones by the insertion of cohesive surfaces between all of the elements in a 2-D analysis, assuming an effective traction-displacement relation between the cohesive surfaces. Transient analyses on initially cracked plates under impact loading showed that the propagation of a crack and its ensuing bifurcation can be qualitatively captured using this method. Camacho and Ortiz (65) also conducted 2-D transient analyses of impact but utilized the adaptive insertion of cohesive zones—that is, a traditional finite element analysis with full connectivity is conducted until an element boundary reaches a specified critical traction, at which time, connectivity is modified, a cohesive “element” is inserted, and the analysis proceeds. This adaptive insertion of cohesive elements prevents some of the wave dispersion effects seen in the Xu and Needleman approach while simultaneously reducing the computational burden by considering less cohesive zones. The method has since

been extended to three dimensions (66). The cohesive zone methods suffer from mesh dependency, both in terms of element size and path dependency. The inherent length scale of the cohesive theory can be used to reduce or even eliminate the mesh-size dependency by computing the process zone size—Falk et al. (67) consider this subject in depth—although the required element size may produce a numerically intractable problem. The mesh path dependency, however, cannot be fully resolved since the fracture must occur along element boundaries, although there is some suggestion that random meshing using triangles/tetrahedra produces a sufficient number of crack paths to reach a converged solution (68, 69). The cohesive zone method has been used to study dynamic fracture along weak planes (70), penetration into brittle materials (65), fragmentation of brittle materials (71), interface crack growth (72), and various other dynamic failure events.

The extended Finite Element Method (XFEM) developed by Belytschko and his coworkers (see Moes et al. [73]) has also proven useful in the simulation of discrete failure in materials. XFEM utilizes enriched nodes (via a partition of unity method) to allow for moving discontinuities in the finite element mesh. As such, crack/discontinuity growth is not limited to element boundaries, and the solution becomes mesh-independent as the overall finite element solution converges. The nodal enrichment in XFEM is problem/constitutive dependent; Moes et al. (73) embedded the square-root singularity from linear elastic fracture mechanics within their formulation. Obviously, changes in constitutive behavior of the material and/or changes in the physics of failure must be directly incorporated in the nodal enrichment. The original 2-D work was extended to three dimensions in Moes et al. (74), and although the extension is nontrivial, the authors demonstrate that three-dimensional (3-D) XFEM crack modeling is possible for elastic and inelastic problems. As the physics for the cracking phenomena must be explicitly represented in the XFEM formulation, XFEM does not account for crack-branching in its standard form; however, researchers have introduced enrichments that allow for branched and intersecting cracks (75).

Song et al. (69) compare XFEM with the cohesive zone method and element deletion, noting that both the XFEM and cohesive zone method can capture dynamic crack propagation, including bifurcation in mode I cracks. Both methods require small elements in the vicinity of the crack tip for convergent solutions—this fact is dictated by the small size of the physical process zone rather than any numerical deficiency. Unlike the continuum damage techniques, XFEM and the cohesive zone method create new surfaces, which are part of their appeal, but they also create more surfaces for the numerical contact algorithms as well. This introduction of additional contact surfaces is particularly relevant in impact/penetration problems where the compressive state of stress places many of the crack faces in contact with one another.

5. Experimental Techniques

The term “dynamic testing” is used quite loosely to cover a wide range of strain rates and testing equipment. Although one would wish to develop material properties for constitutive relationships to describe a material’s behavior across a wide spectrum of strain rates, that may not usually be the case in general. This is to be expected because the dominant deformation mechanism of a material may change from one strain rate regime to another. Figure 9 is a good summary of the various dynamic characteristics associated with mechanical testing (76).

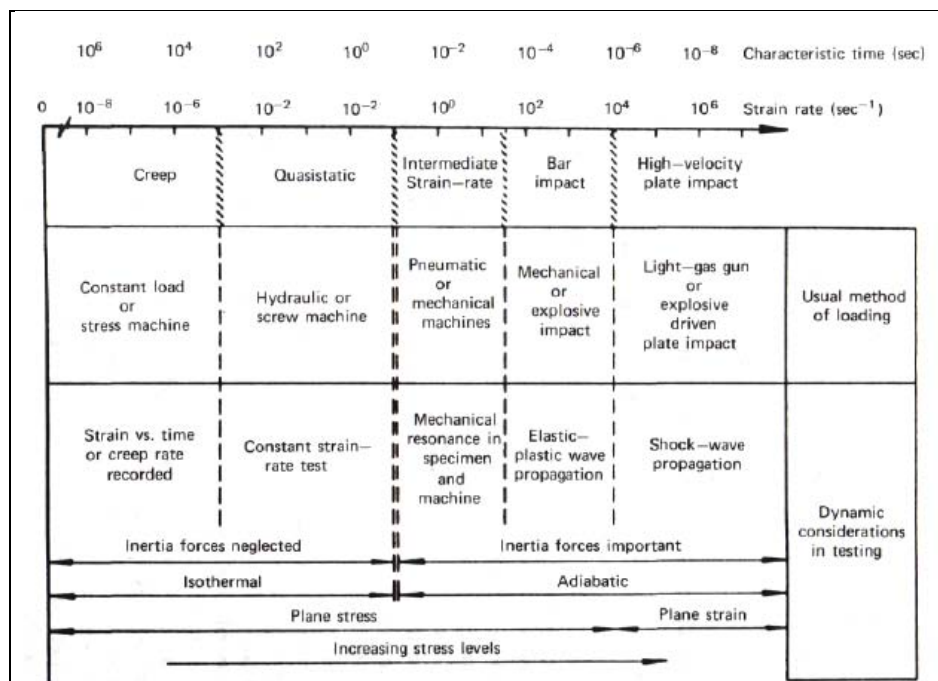


Figure 9. Dynamic aspects associated with mechanical testing (76).

5.1 Plate Impact

Here we discuss gas gun driven plate impact experiments of condensed matter (the methodology described here is generalized). The primary objective of a plate impact experiment is to generate a planar shock compression wave in a uniaxial state of strain in the target material. This is normally attained by the use of gas guns (single stage, two stage, powder, or electromagnetic), explosives, or lasers, depending on the strain rate of interest. With the use of a gas gun, a flyer plate mounted on a sabot is driven into a target, resulting in a symmetric or non-symmetric impact, depending on the flyer and target material. If the flyer and target material are identical, then the impact is said to be symmetric; otherwise, it is non-symmetric. A series of charged pins

is used to determine the flyer velocity prior to impacting the target. For a test to be considered acceptable, the impact between the flyer and the target must be parallel to within 2 mrad. The lateral dimensions of the specimens are chosen so that uniaxial strain condition is maintained throughout the time of interest, during which free surface velocity measurements are made. In other words, free surface velocity measurements are made prior to the arrival of the radial release waves. Upon impact, a two-structure shock compression wave is generated at the impact interface, traveling in opposite direction as shown in figure 10 (a), the time-distance or Lagrangian plot. The two-structure shock compression wave comprises an elastic wave and a slower plastic wave. At time t_1 , the first time-of-arrival signal for the elastic wave is detected by the Velocity Interferometer System for Any Reflector (VISAR [77]) at the free surface of the target and shortly thereafter at time t_2 that of the plastic wave is detected.

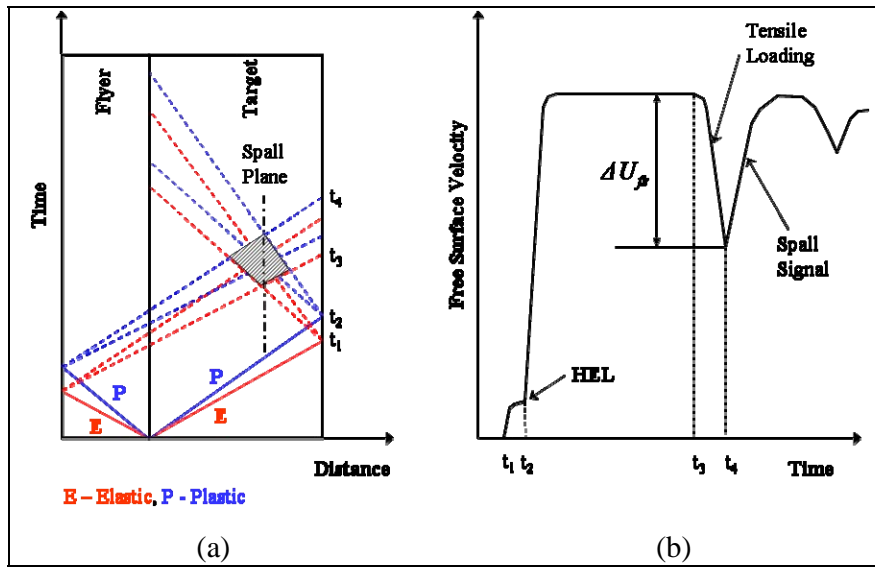


Figure 10. (a) Lagrangian or time-distance diagram and (b) the velocity-time history of a two-structure wave.

Both waves are reflected as rarefaction waves. Similarly, the two-structure shock compression wave in the flyer specimen is reflected at the free surface as a rarefaction wave. Assuming a symmetric impact, both elastic and plastic rarefaction waves from the flyer free surface are completely transmitted through the impact interface into the target material. When the rarefaction waves from both free surfaces interact, a region of almost pure hydrostatic tension is generated, and stresses that are greater than the threshold stress required for damage initiation are produced, as shown in figure 10 (a). Within this region, voids nucleate, grow, and coalesce to form well-defined spall damage in ductile materials and can result in material failure. A good review of the plate impact technique has been compiled by Fowles et al. (78).

The discovery of lasers has led to the invention of optical interferometry, which currently is the most powerful tool in the determination of the surface motion of shocked condensed matter. A schematic representation of the velocity-time history of a plate impact experiment is shown in

figure 10 (b). Acquiring the velocity-time history is of the utmost importance in spall fracture experiments. Useful experimental information such as the Hugoniot Elastic Limit (HEL), plastic rise time, peak pressure (related to the maximum velocity, V_{\max}), pull-back velocity (ΔU_{fs}), etc., can be extracted from the velocity-time history. The HEL is defined as the point at which a solid, loaded in compression under the constraint of uniaxial strain, can no longer support elastic distortion and begins to flow through plastic or cataclastic (crushing) fracture processes (79). Also, the spall strength is directly related to the pull-back velocity by the relationship

$$\sigma^* = \frac{1}{2} \rho_0 c_0 \Delta U_{fs} , \quad (17)$$

where σ^* is the spall strength, ρ_0 is the density of the material, and C_0 is the bulk sound speed. Acquiring the velocity-time history from a plate impact experiment requires a VISAR. The VISAR has been one of the most important breakthroughs in experimental shock physics of condensed matter. The VISAR is an extension of the Michelson Interferometer, and the working principles are based on Doppler shift, i.e., due to the movement of the free surface of the target specimen, the system produces interference fringe shifts that are proportional to the Doppler shift of the laser light. Because of the importance of VISAR in experimental shock physics, its operation is discussed in the following paragraphs. A schematic of the VISAR system is shown in figure 11. The impact between the flyer and target takes place inside a vacuum chamber, as shown in the figure. A laser beam is focused on the back free surface of the target, and the reflected light is collimated and then split into two beams by a 10–90 beam splitter, i.e., 10% reflected and 90% transmitted. The 10% reflected beam is directed to a Beam Intensity Monitor (BIM) for monitoring and diagnostic purposes. The 90% transmitted beam is further split into a reference leg and a delay leg by a 50–50 beam splitter. The delay leg is achieved by transmitting the beam through a glass etalon (fused silica) and then shifted by a $\lambda/8$ wave plate. The purpose of the delay is to achieve a 90° phase difference between the two beams. The physical distances traveled by the reference and delay legs are made to be equivalent to within a few thousandths of an inch in order to obtain quality fringe patterns. Both legs are then separated into S and P components of light by a Polarizing Beam Splitter (PBS) and then recombined to form two 90° out-of-phase signals that are sinusoidal in nature. These fringes are shifted whenever the free surface of the target is accelerated, and surface velocity $V(t)$ is related to the total fringe count $F(t)$ by the equation

$$V(t - \frac{1}{2} \tau) = \frac{\lambda}{2\tau} \frac{F(t)}{(1 + \delta)(1 + \Delta v / v)} , \quad (18)$$

where λ is the wavelength of the laser beam, δ is a correction factor due to the wavelength dependence of the refractive index on the etalon, and $\Delta v / v$ is an optical correction term.

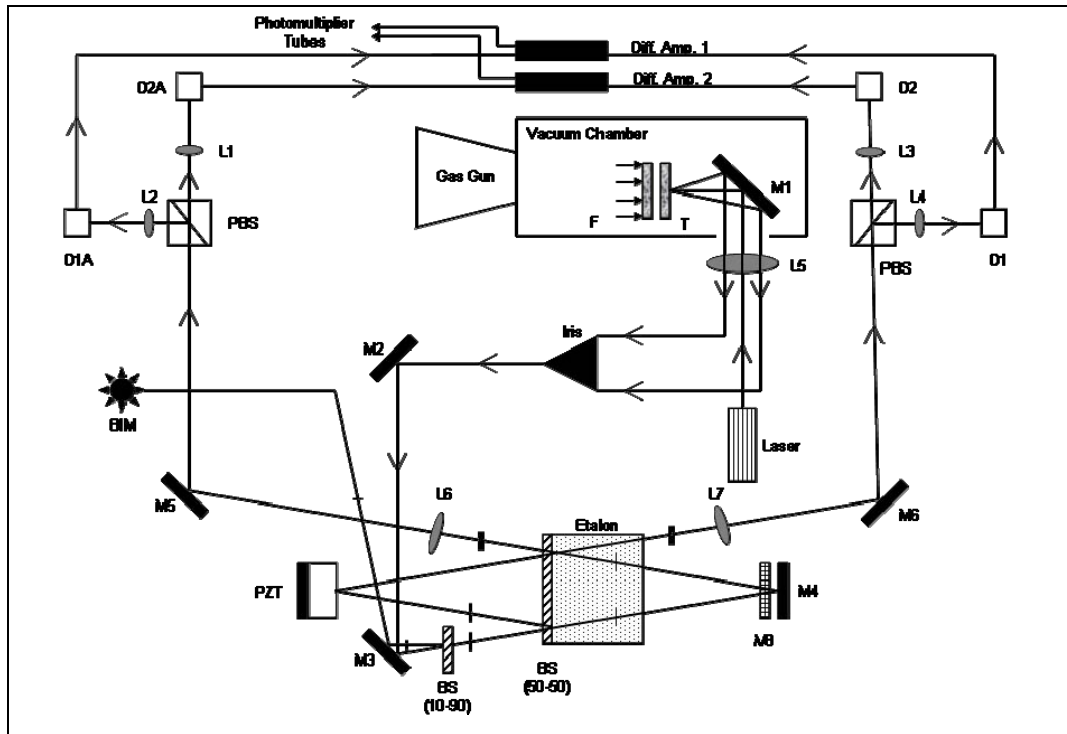


Figure 11. A schematic representation of the VISAR system.

5.2 Dynamic Fracture

Experimental techniques to elucidate dynamic fracture have taken many forms over the past 50 years, but all focus on the ability to discern the crack speed and, more recently, the state of stress/strain in the vicinity of the crack tip. Techniques can generally be classified as optical and non-optical, with current research trending toward optical methods (due to their ability to capture full-field information).

Non-optical methods for dynamic fracture can be further subdivided into stress wave/crack interaction and electrical resistance methods. Wallner (80) discovered that during crack propagation, the interaction between a propagating crack and shear waves produced during the fracture process produced distinct ridges in the fracture surface. In a postmortem analysis, one can use these ridges (along with the shear wave speed in the material) to estimate the crack velocity.

Ravi-Chandar (53) gives an excellent review of the technical details of these “Wallner lines” and how they can be used to measure the crack speed. Kerkhof (9) extended this method by introducing an ultrasonic transducer as a source of shear waves; now the creation of the Wallner lines is governed by a user-controlled frequency, thus appearing as smooth “ripples” on the crack surface with a specified temporal frequency. Their spatial frequency can then be used to determine the crack speed with a high degree of accuracy. This so-called “stress wave

fractography” is discussed in detail in Richter and Kerkhof (81). Kerkhof (9) used this method to find the speed of cracks in glasses with a 1-MHz transducer, allowing the accurate determination of crack speeds up to 2000 m/s.

Electrical resistance methods rely on sets or grids of fine electrical wires applied to the material of interest. As the crack passes, each wire is broken, providing a direct crack position as a function of time. Many researchers have utilized this technique—possibly the first being Dulaney and Brace (82)—and the grids are now commercially available. Thin films coupled with alternating currents can also be utilized to determine crack velocities (83) at a high sampling rate when great care is taken to prepare the thin film and measure its resistance changes as the crack propagates.

Optical techniques utilizing high-speed cameras are some of the most prominent dynamic fracture instrumentation techniques. Crack propagation speeds in excess of 1 km/s require the use of cameras with very high framing rates to capture fracture processes in situ. Schardin (6) developed a spark camera (now frequently referred to as the Cranz-Schardin camera) that utilizes a set of light sources and lenses that produces separate images for the pulse of each light source; thus framing rates approaching 1 million frames per second can be obtained, as the exposure time is independent of the framing rate. Lu and Liu (84) offer a review of the construction of Cranz-Schardin cameras, discussing the original spark-based system as well as a modern Light Emitting Diode (LED) system. Rotating mirror cameras can improve the temporal frequency, approaching 5 million frames per second, while still retaining excellent image quality. Gated intensified cameras utilize beam splitting optics and Charged Coupled Device (CCD) arrays to generate extremely high framing rates (>200 million frames per second) for a limited number of frames at very short exposure times (<5 ns) with reduced image quality as compared to rotating mirror cameras. Recently, several manufacturers have developed single CCD video cameras capable of framing rates in excess of 1 million frames per second with excellent image quality for dozens, if not hundreds, of frames. Regardless of the camera type, several imaging techniques have been utilized by researchers to gain insight into dynamic fracture.

Direct high speed photography grants some information about the propagation of cracks in transparent materials, but other techniques are often employed that give additional information. The shadowgraph method frequently referred to as the method of caustics (85) utilizes the local slope change (opaque, reflective materials) or the thickness change (transparent materials) near the crack tip to produce a shadow “spot” that precisely locates the crack tip during a dynamic event. Detailed analyses by Kalthoff (86) show that one can use the size and shape of this spot to determine the relative magnitude of the loading and the mode mixity of the crack, respectively. An example of an LECEI test for PMMA is shown in figure 12 (87).

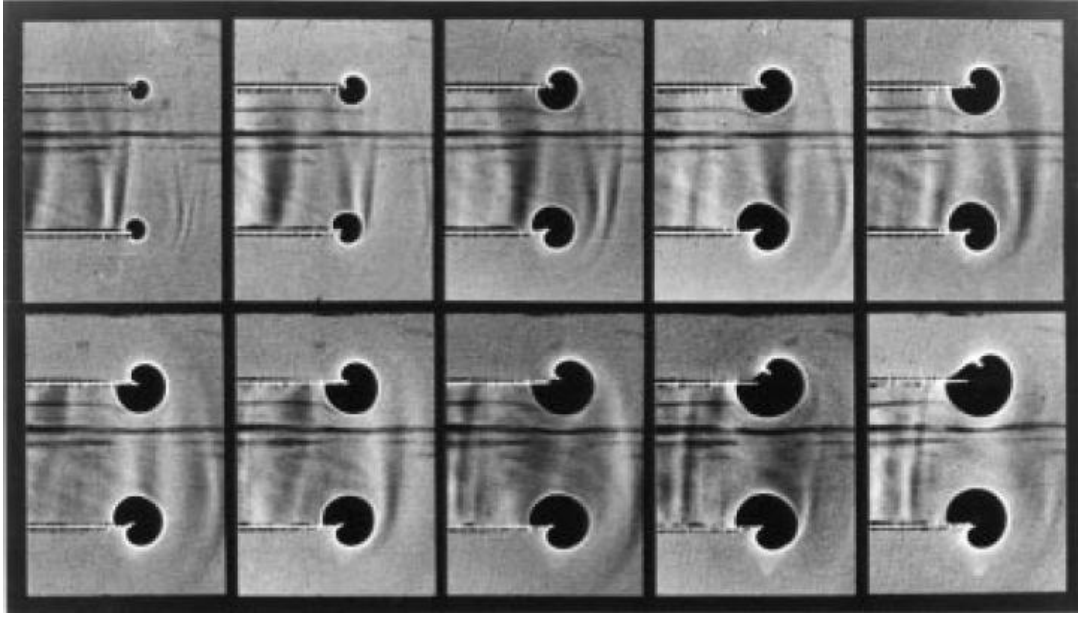


Figure 12. Method of caustics applied to edge-impacted pre-cracked PMMA specimen, resulting in mode-II dominant cracks (87).

Tippur et al. (88) introduced an interferometric technique that measures gradients of the out-of-plane surface displacements, naming the technique coherent gradient sensing (CGS). This method has proven to be quite useful for dynamic crack propagation; it is relatively insensitive to vibrations, entirely insensitive to rigid body motions, and the resulting fringe patterns can distinguish the mode mixity of the crack through comparison to analytical solutions. The full-field information allows critical examination of crack bifurcation, including shifts in mode-mixity or failure type (such as a shift to adiabatic shear banding [89]). Furthermore, a slight change in experimental setup allows the technique to be applied to either transparent or specularly reflective materials. Figure 13 shows the optical setup for reflective CGS; details of the analysis technique can be found in Tippur (90). The technique uses a coherent light source and a set of carefully aligned Ronchi rulings to create a series of fringe-based images; a lens is used to focus each image to a small enough size such that an aperture can isolate the image of interest. The $+1/-1$ images (the first image above and below the optical axis) produce the gradient of the out-of-plane displacement in the direction of the Ronchi rulings; obviously, the Ronchi rulings can be rotated to give different gradients as desired.

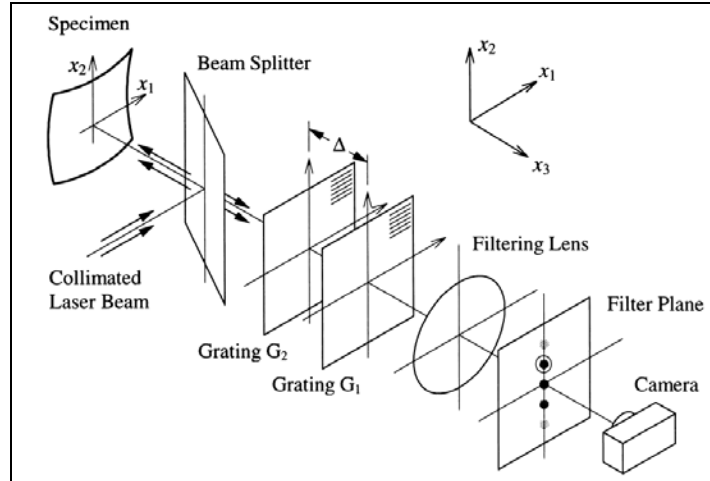


Figure 13. Diagram of coherent gradient sensing experimental setup for reflective materials (from Rosakis et al. [91]).

CGS has been successfully employed to study the fracture behavior of metals (48), metallic glasses (92), fiber-reinforced composites (93), and polymers (94); indeed the method is applicable to any material with sufficient local deformation at the crack tip. CGS is difficult to employ for materials with extremely small strains at fracture (e.g., borosilicate glass)—the small strain gradients produce too few fringes to reliably measure. While not a limitation of the technique, the amount of light required for high-speed photography dictates a significantly powerful laser with a long coherence length (argon-ion and diode-pumped solid state lasers of approximately 10 W have been used with exposure times of approximately 0.5 μ s). Other optical techniques have been utilized to measure deformations of the sample in an attempt to monitor dynamic crack propagation. Digital image correlation (DIC) (95) utilizes a random speckle pattern and one or more high-speed cameras to track the motion of the speckles and produce a deformation field of the sample. A single camera can track in-plane deformations; adding a second with an appropriate angle can possibly allow 3-D tracking. DIC has been very successfully employed in tracking strain behavior of materials and deformations of structures; crack propagation tests the method because of the very small opening displacements, particularly near the crack tip. Direct interferometric measurement of the out-of-plane displacements has been employed by numerous researchers (e.g., Kalthoff [87]) for dynamic crack propagation. Given that this measurement relies on the wavelength of the coherent light source (frequently approximately 500 nm), the resulting fringe pattern captures very small deformations. While quite useful, setup and post-processing can be difficult as the method is sensitive to initial alignment and rigid body rotations.

6. Concluding Remarks

The understanding, characterization, and simulation of dynamic failure of materials are critical for military weapons research; areas such as warhead fragmentation, penetration of brittle armors, and projectile breakup are controlled by material failure and its kinetics. This knowledge also impacts civilian applications, such as fragmentation of rocks for mineral and oil extraction, protection of space vehicles from cosmic debris impact, barricade design for civil structures. The presented review shows the advancements in dynamic failure research including failure modes ranging from spallation to brittle fracture over the past 50 years. Experimental techniques, theoretical models, and computational methods for dynamic failure were discussed, giving a historical state-of-the-art perspective on work performed in this area.

While there is an abundance of work in the field, several key topics resonated with the authors for the focus of future work. Experimental methods are trending toward higher resolution in both space and time; full-field and/or penetrative (X-ray/proton radiography) imaging in situ can give some indication of the kinetics of dynamic failure that is not apparent from postmortem examination. These experiments can provide some needed verification/validation for both old and new models for dynamic failure. Numerical modeling techniques for dynamic failure are becoming more sophisticated (e.g., extended finite element and cohesive zone methods) rather than the traditional continuum damage mechanics approaches. This trend should help material modelers better represent failure and failed material, as there is now a numerical representation of the evolving surfaces—a critical step to correctly modeling wave propagation and local stress states. It is currently unknown how well the current trend of multi-scale modeling will impact dynamic failure; however, it could potentially help link smaller-scale processes, such as dislocation dynamics, grain-to-grain interface failure, and pre-existing microstructural flaws to the nucleation and propagation of macro-scale cracks. Invariably, the materials science and mechanics communities will need close collaboration to reach a fundamental understanding of the dynamic failure of materials, a difficult but rewarding goal to achieve.

7. References

1. Freund, L. B. Crack Propagation in an Elastic Solid Subjected to General Loading—3. Stress Wave Loading. *J. Mech. Phys. Solids* **1973**, *21*, 47–61.
2. Griffith, A. A. The Phenomenon of Rupture and Flow in Solids. *Philos. Trans. R. Soc. London, Ser. A* **1920**, *A221*, 163–198.
3. Mott, N. F. Brittle Fracture in Mild Steel Plates. *Engineering* **1948**, *165*, 16–18.
4. Irwin, G. R. Fracture Dynamics. *Fracturing of Metals*; American Society of Metals: Cleveland, OH, 1948; pp 147–166.
5. Irwin, G. R. Analysis of Stresses and Strains Near the End of a Crack Traversing a Plate. *J. Appl. Mech.* **1957**, *24*, 361–364.
6. Schardin, H. Velocity Effects in Fracture. In *Fracture*; Averbach, B. L., Ed.; MIT Press: Cambridge, MA, 1959; pp 297–330.
7. Edgerton, H. E.; Barstow, F. E. Further Studies of Glass Fracture With High-Speed Photography. *J. Am. Ceram. Soc.* **1941**, *24*, 131–137.
8. Kerkhof, F. *Bruchvorgänge in Glasern*; Verlag der Deutschen Glastechnischen Gesellschaft: Frankfurt, Germany, 1970.
9. Kerkhof, F. Wave Fractographic Investigations of Brittle Fracture Dynamics. In *Dynamic Crack Propagation*; Sih, G. C., Ed.; Noordhoff: Leyden, The Netherlands, 1973; pp 3–35.
10. Kobayashi, A. S.; Chan, C. F.; A Dynamic Photoelastic Analysis of Dynamic Tear Test Specimen. *Exp. Mech.* **1976**, *16*, 176–181.
11. Manogg, P. Investigation of the Rupture of a Plexiglass Plate by Means of an Optical Method Involving High Speed Filming of the Shadows Originating Around Holes Drilled in the Plate. *Int. J. Fracture* **1966**, *2*, 604–613.
12. Wells, A. A.; Post, D. The Dynamic Stress Distribution Surrounding a Running Crack—A Photoelastic Analysis. *Proc. SESA* **1958**, *16*, 69–92.
13. Kolsky, H. *Stress Waves in Solids*; Dover: Mineola, NY, 1953.
14. Dally, J. W. Dynamic Photoelasticity and its Application to Stress Wave Propagation, Fracture Mechanics, and Fracture Control. In *Static and Dynamic Photoelasticity and Caustics*; Largarde, A., Ed.; Springer-Verlag: New York, 1987; pp 247–406.

15. Kalthoff, J. F. The Shadow Optical Method of Caustics. In *Static and Dynamic Photoelasticity and Caustics*; Largarde, A., Ed.; Springer-Verlag: New York, 1987; pp 407–552.
16. Hopkinson, B. Effects of the Detonation of Gun Cotton. *Proc. R. Soc. London* **1914**, A89, 411–413.
17. Rinehart, J. S.; Pearson, J. *Behavior of Metals Under Impulsive Loads*; American Society for Metals: Dover, NY, 1964.
18. Stevens, A. L.; Tuler, F. R. Effect of Shock Precompression on Dynamic Fracture Strength of 1020 Steel and 6061-T6 Aluminum. *J. Appl. Phys.* **1971**, 42, 5665.
19. Buchanan, J.; James, H. Measurement of High Intensity Stress Pulses. *Br. J. Appl. Phys.* **1959**, 10, 290–295.
20. Davison, L.; Stevens, A. L. Continuum Measures of Spall Damage. *J. Appl. Phys.* **1972**, 43, 988.
21. Davison, L.; Stevens, A. L. Thermomechanical Constitution of Spalling Elastic Bodies. *J. Appl. Phys.* **1973**, 44, 668.
22. Davison, L.; Stevens, A. L.; Kipp, M. E. Theory of Spall Damage Accumulation in Ductile Metals. *J. Mech. Phys. Solids* **1977**, 25, 11–28.
23. Meyers, M. A., Murr, L. E., Eds. *Shock Waves and High-Strain Rate Phenomena in Metals: Concepts and Applications*; Plenum Press: New York, 1981.
24. Mott, N. F. Fragmentation of Shell Cases. *Proc. R. Soc. London* **1947**, 189, 300–308.
25. Grady, D. Local Inertial Effects in Dynamic Fragmentation. *J. Appl. Phys.* **1982**, 53, 322–325.
26. Wesenberg, D. L.; Sagartz, M. J. Dynamic Fracture of 6061-T6 Aluminum Cylinders. *J. Appl. Mech.* **1977**, 44, 643.
27. Hertzberg, R. W. *Deformation and Fracture Mechanics of Engineering Materials*; J. Wiley: New York, 1976; pp 273, 341.
28. Curran, D. R. In *Shock Waves and the Mechanical Properties of Solids*; Burke, J. J., Weiss, V., Eds.; Syracuse University Press: New York, 1971; p 121.
29. Barbee, T. W.; Seaman, L.; Crewdson, R.; Curran, D. Dynamic Fracture Criteria for Ductile and Brittle Metals. *J. Mater. JMLSA* **1972**, 7, 393–401.
30. Seaman, L.; Shockey, D. A.; Curran, D. R. In *Dynamic Crack Propagation*; Sih, G. C., Ed.; Noordhoff: Leyden, The Netherlands, 1973; p 629.

31. Curran, D. R.; Shockey, D. A.; Seaman, L. Dynamic Fracture Criteria for a Polycarbonate. *J. Appl. Phys.* **1973**, *44*, 4025–4038.
32. Shockey, D. A.; Seaman, L.; Curran, D. R.; source cited in ref. 28, p. 473.
33. Seaman, L.; Curran, D. R.; Shockey, D. A. Computational Models for Ductile and Brittle Fracture. *J. Appl. Phys.* **1976**, *47*, 4814–4826.
34. Curran, D. R.; Seaman, L.; Shockey, D. A. Dynamic Failure in Solids. *Phys. Today* **1977**, *30*, 46.
35. Shockey, D. A.; Curran, D. R.; Seaman, L. In *High Velocity Deformation of Solids*; Kawata, K., Shiori, J., Eds.; Springer-Verlag: Berlin, Germany, 1979; p 149.
36. Seaman, L.; Curran, D. R.; Crewdson, R. C. Transformation of Observed Crack Traces on a Section to True Crack Density for Fracture Calculations. *J. Appl. Phys.* **1978**, *49*, 5221–5229.
37. McClintock, F. A. A Criterion for Ductile Fracture by the Growth of Holes. *J. Appl. Mech.* **1968**, *35*, 363–371.
38. McClintock, F. A. Local Criteria for Ductile Fracture. *Int. J. Fract. Mech.* **1968**, *4*, 101–130.
39. Rice, J. R.; Tracey, D. M. On Ductile Enlargements of Voids in Triaxial Stress Fields. *J. Mech. Phys. Solids* **1969**, *17*, 201.
40. Needleman, A. Void Growth in an Elastic-Plastic Medium. *J. Appl. Mech.* **1972**, *39*, 964–970.
41. Yoffe, E. H. The Moving Griffith Crack. *Philos. Mag.* **1951**, *42*, 739–750.
42. Baker, B. R. Dynamic Stress Created by a Moving Crack. *J. Appl. Mech.* **1962**, *29*, 449–458.
43. Freund, L. B. *Dynamic Fracture Mechanics*; Cambridge University Press: Cambridge, Massachusetts, 1990.
44. Ravi-Chandar, K.; Knauss, W. G. An Experimental Investigation Into Dynamic Fracture, Part 1: Crack Initiation and Arrest. *Int. J. Fracture* **1984**, *25*, 247–262.
45. Ravi-Chandar, K.; Knauss, W. G. An Experimental Investigation Into Dynamic Fracture, Part 2: Microstructural Aspects. *Int. J. Fracture* **1984**, *26*, 65–80.
46. Ravi-Chandar, K.; Knauss, W. G. An Experimental Investigation Into Dynamic Fracture, Part 3: On Steady-State Crack Propagation and Crack Branching. *Int. J. Fracture* **1984**, *26*, 141–154.

47. Ravi-Chandar, K.; Knauss, W. G. An Experimental Investigation Into Dynamic Fracture, Part 4: On the Interaction of Stress Waves With Propagating Cracks. *Int. J. Fracture* **1984**, *26*, 189–200.
48. Pandolfi, A.; Guduru, P. R.; Ortiz, M.; Rosakis, A. J. Three Dimensional Cohesive-Element Analysis and Experiments of Dynamic Fracture in C300 Steel. *Int. J. Solids Struct.* **2000**, *37*, 3733–3760.
49. Kalthoff, J.; Winkler, S. Failure Mode Transition of High Rates of Shear Loading. In *Proceedings of the International Conference on Impact Loading and Dynamic Behavior of Materials*; Chiem, C. Y., Kunze, H.-D., Meyer, L. W., Eds.; Deutsche Gesellschaft fure Metallkunde, DGM-Verlag: Bremen, Oberursel, 18–22 May 1987.
50. Zhou, M.; Ravichandran, G.; Rosakis, A. J. Dynamically Propagating Shear Bands in Impact Loaded Prenotched Plates. *J. Mech. Phys. Solids* **1996**, *44*, 981–1032.
51. Rosakis, A. J.; Samudrala, O.; Coker, D. Cracks Faster Than the Shear Wave Speed. *Science* **1999**, *284*, 1337–1340.
52. Rosakis, A. J.; Intersonic Shear Cracks and Fault Ruptures. *Adv. Phys.* **2002**, *51*, 1189–1257.
53. Ravi-Chandar, K. *Dynamic Fracture*; Elsevier Science: Amsterdam, The Netherlands, 2004.
54. Kachanov, L. M. On Creep Rupture Time. *Izv. Acad. Nauk SSSR, Otd. Techn. Nauk.* **1958**, *8*, 26–31.
55. Johnson, G. R.; Cook, W. H. Fracture Characteristics of Three Metals Subjected to Various Strains, Strain Rates, Temperatures, and Pressures. *Eng. Fract. Mech.* **1985**, *21*, 31–48.
56. Gurson, A. L. Continuum Theory of Ductile Rupture by Void Nucleation and Growth, Part I. *J. Eng. Mater. Tech.* **1977**, *99*, 2–15.
57. Johnson, J. N.; Addessio, F. L. Tensile Plasticity and Ductile Fracture. *J. Appl. Phys.* **1988**, *64*, 6699–6712.
58. Addessio, F. L.; Johnson, J. N. Rate-Dependent Ductile Failure Model. *J. Appl. Phys.* **1993**, *74*, 1640–1648.
59. Rajendran, A. M.; Grove, D. J. Modeling the Shock Response of Silicon Carbide, Boron Carbide and Titanium Diboride. *Int. J. Impact Eng.* **1996**, *18*, 611–631.
60. Johnson, G. R.; Holmquist, T. J. Response of Boron Carbide Subjected to Large Strains, High Strain Rates and High Pressures. *J. Appl. Phys.* **1999**, *85*, 8060–8073.

61. Mayes, J. S.; Hansen, A. C. Multicontinuum Failure Analysis of Composite Structural Laminates. *Mech. Comp. Mat. Struct.* **2001**, 8, 249–262.
62. Dugdale, D. S. Yielding of Steel Sheets Containing Slits. *J. Mech. Phys. Solids* **1960**, 8, 100–104.
63. Barenblatt, G. I. The Mathematical Theory of Equilibrium of Cracks in Brittle Fracture. *Adv. Appl. Mech.* **1962**, 7, 55–129.
64. Xu, X.-P.; Needleman, A. Numerical Simulations of Fast Crack Growth in Brittle Solids. *J. Mech. Phys. Solids* **1994**, 42, 1397–1434.
65. Camacho, G. T.; Ortiz, M. Computational Modeling of Impact Damage in Brittle Materials. *Int. J. Solids Structures* **1996**, 33, 2899–2938.
66. Ortiz, M.; Pandolfi, A. Finite-Deformation Irreversible Cohesive Elements for Three-Dimensional Crack-Propagation Analysis. *Int. J. Numer. Meth. Eng.* **1999**, 44, 1267–1282.
67. Falk, M. L.; Needleman, A.; Rice, J. R. A Critical Evaluation of Cohesive Zone Models of Dynamic Fracture. *Journal de Physique IV, Proceedings* **2001**, 5, 5.43–5.50.
68. Molinari, J. F.; Gazonas, G.; Raghupathy, R.; Rusinek, A.; Zhou, F. The Cohesive Element Approach to Dynamic Fragmentation: The Question of Energy Convergence. *Int. J. Numer. Meth. Eng.* **2006**, 69, 484–503.
69. Song, J.-H.; Wang, H.; Belytschko, T. A Comparative Study on Finite Element Methods for Dynamic Fracture. *Comput. Mech.* **2008**, 42, 239–250.
70. Arias, I.; Knap, J.; Chalivendar, V. B.; Hong, S.; Ortiz, M.; Rosakis, A. J. Numerical Modeling and Experimental Validation of Dynamic Fracture Events Along Weak Planes. *Comput. Methods Appl. Mech. Engrg.* **2007**, 196, 3833–3840.
71. Espinosa, H. D.; Zavattieri, P. D.; Dwivedi, S. K.; A Finite Deformation Continuum/Discrete Model for the Description of Fragmentation and Damage in Brittle Materials. *J. Mech. Phys. Solids* **1998**, 46, 1909–1942.
72. Tvergaard, V. Predictions of Mixed Mode Interface Crack Growth Using a Cohesive Zone Model for Ductile Fracture. *J. Mech. Phys. Solids* **2004**, 52, 925–940.
73. Moes, N.; Dolbow, J.; Belytschko, T. A Finite Element Method for Crack Growth Without Remeshing. *Int. J. Numer. Meth. Engng.* **1999**, 46, 131–150.
74. Moes, N.; Gravouil, A.; Belytschko, T. Non-Planar 3D Crack Growth by the Extended Finite Element and Level Sets – Part I: Mechanical Model. *Int. J. Numer. Meth. Engng.* **2002**, 53, 2549–2568.

75. Daux, C.; Moes, N.; Dolbow, J.; Sukumar, N.; Belytschko, T. Arbitrary Branched and Intersecting Cracks With the Extended Finite Element Method. *Int. J. Numer. Meth. Engng.* **2000**, *48*, 1741–1760.
76. Lindholm, U. S. High Strain Testing, Part 1: Measurement of Mechanical Properties. In *Techniques in Metals Research*; Bunshah, R. F., Ed.; Interscience: New York, 1971; Vol. 5, Part 1.
77. Barker, L. M.; Hollenbach, R. E. Laser Interferometer for Measuring High Velocities of Any Reflecting Surface. *J. Appl. Phys.* **1972**, *43*, 4669–4675.
78. Fowles, G. R.; Duvall, G. E.; Asay, J.; Bellamy, P.; Feistmann, F.; Grady, D.; Micheals, T.; Mitchell, R. Gas Gun for Impact Studies. *Rev. Sci. Instrum.* **1970**, *41*, 984.
79. Grady, D. E. Shock-Wave Properties of High-Strength Ceramics. In *Shock Compression of Condensed Matter-1991*; Elsevier Science: Amsterdam, The Netherlands, 1991.
80. Wallner, H. Linienstrukturen an Bruchflächen. *Z. Physik* **1938**, *114*, 739–750.
81. Richter, H. G.; Kerkhof, F. Stress Wave Fractography. In *Fractography of Glass*; Bradt, R. C., Tressler, R. E., Eds.; Plenum Press: New York, 1994.
82. Dulaney, E. N.; Brace, W. F. Velocity Behavior of a Growing Crack. *J. Appl. Phys.* **1960**, *31*, 2233–2236.
83. Fineberg, J.; Gross, S. P.; Marder, M.; Swinney, H. L. Instability in the Propagation of Fast Cracks. *Phys. Rev. B* **1992**, *45*, 5146–5154.
84. Lu, F. K.; Liu, X. Optical Design of Cranz-Schardin Cameras. *Opt. Eng.* **1997**, *36*, 1935–1941.
85. Theocaris, P. S. Reflected Shadow Method for Study of Constrained Zones in Cracked Plates. *Appl. Opt.* **1971**, *10*, 2240.
86. Kalthoff, J. F.; Shadow Optical Method of Caustics. In *Handbook on Experimental Mechanics*, 2nd ed.; Kobayashi, A. S., Ed.; VCH Publishers: New York, 1993; Chapter 9, pp 407–476.
87. Kalthoff, J. F. Modes of Dynamic Shear Failure in Solids. *Int. J. Fracture*, **2000**, *101*, 1–31.
88. Tippur, H. V.; Krishnaswamy, S.; Rosakis, A. J. A Coherent Gradient Sensor for Crack Tip Deformation Measurements: Analysis and Experimental Results. *Int. J. Fracture* **1991**, *48*, 193–204.

89. Mason, J. J.; Rosakis, A. J.; Ravichandran, G. Full Field Measurements of the Dynamic Deformation Field Around a Growing Adiabatic Shear Band at the Tip of a Dynamically Loaded Crack or Notch. *J. Mech. Phys. Solids* **1994**, *42*, 1679–1697.
90. Tippur, H. V.; Coherent Gradient Sensing: A Fourier Optics Analysis and Applications to Fracture. *Appl. Opt.* **1992**, *31*, 4428–4439.
91. Rosakis, A. J.; Singh, R. P.; Tsuji, Y.; Kolawa, E.; Moore, N. R., Jr. Full Field Measurements of Curvature Using Coherent Gradient Sensing: Application to Thin Film Characterization. *Thin Solid Films* **1998**, *325*, 42–54.
92. Rittel, D.; Rosakis, A. J. Dynamic Fracture of Beryllium-Bearing Bulk Metallic Glass Systems: A Cross-Technique Comparison. *Eng. Frac. Mech.* **2005**, *72*, 1905–1919.
93. Liu, C.; Rosakis, A. J.; Ellis, R. W.; Stout, M. G. A Study of the Fracture Behavior of Unidirectional Fiber-Reinforced Composite Using Coherent Gradient Sensing (CGS) Interferometry. *Int. J. Fracture* **1998**, *90*, 355–382.
94. Xu, W.; Yao, X. F.; Yeh, H. Y.; Gin, G. C. Fracture Investigation of PMMA Specimen Using Coherent Gradient Sensing (CGS) Technology. *Polym. Test.* **2005**, *24*, 900–908.
95. Bruck, H. A.; McNeill, S. R.; Sutton, M. A.; Peters, W. H. Digital Image Correlation Using Newton-Raphson Method of Partial-Differential Correction. *Exp. Mech.* **1989**, *29*, 261–267.

NO. OF
COPIES ORGANIZATION

1 DEFENSE TECHNICAL
(PDF INFORMATION CTR
only) DTIC OCA
8725 JOHN J KINGMAN RD
STE 0944
FORT BELVOIR VA 22060-6218

1 DIRECTOR
US ARMY RESEARCH LAB
IMNE ALC HRR
2800 POWDER MILL RD
ADELPHI MD 20783-1197

1 DIRECTOR
US ARMY RESEARCH LAB
RDRL CIM L
2800 POWDER MILL RD
ADELPHI MD 20783-1197

1 DIRECTOR
US ARMY RESEARCH LAB
RDRL CIM P
2800 POWDER MILL RD
ADELPHI MD 20783-1197

1 DIRECTOR
US ARMY RESEARCH LAB
RDRL D
2800 POWDER MILL RD
ADELPHI MD 20783-1197

ABERDEEN PROVING GROUND

1 DIR USARL
RDRL CIM G (BLDG 4600)

NO. OF
COPIES ORGANIZATION

1 (CD ONLY) DPTY ASSIST SCT FOR R&T
SARD TT
ASA ACT
J PARMENTOLA
THE PENTAGON RM 3E479
WASHINGTON DC 20310-1714

1 PRIN DPTY FOR TCHNLGY HQ
US ARMY MATCOM
AMCDCGR
R PRICE
9301 CHAPEK RD
FT BELVOIR VA 22060-5527

3 AIR FORCE ARMAMENT LAB
AFATL DLJW
W COOK
D BELK
J FOSTER
EGLIN AFB FL 32542

2 NSF
S MCKNIGHT
G PAULINO
4201 WILSON BLVD STE 545
ARLINGTON VA, 22230-0002

1 DARPA
W COBLENZ
3701 N FAIRFAX DR
ARLINGTON VA 22203-1714

1 DIRECTOR
US ARMY TACOM ARDEC
AMSRD AAR AEE W
E BAKER
BLDG 3022
PICATINNY ARSENAL NJ
07806-5000

2 US ARMY TARDEC
AMSTRA TR R MS 263
K BISHNOI
D TEMPLETON MS 263
WARREN MI 48397-5000

1 COMMANDER
US ARMY RSRCH OFC
RDRL ROE N
B LAMATTINA
PO BOX 12211
RESEARCH TRIANGLE PARK NC
27709-2211

NO. OF
COPIES ORGANIZATION

1 COMMANDER
US ARMY RSRCH OFC
RDRL ROI M
J LAVERY
PO BOX 12211
RESEARCH TRIANGLE PARK NC
27709-2211

1 COMMANDER
US ARMY RSRCH OFC
RDRL ROE M
D STEPP
PO BOX 12211
RESEARCH TRIANGLE PARK NC
27709-2211

5 NAVAL RESEARCH LAB
E R FRANCHI CODE 7100
M H ORR CODE 7120
J A BUCARO CODE 7130
J S PERKINS CODE 7140
S A CHIN BING CODE 7180
4555 OVERLOOK AVE SW
WASHINGTON DC 20375

1 DTRA
M GILTRUD
8725 JOHN J KINGMAN RD
FORT BELVOIR VA 22060

1 ERDC
US ARMY CORPS OF ENGINEERS
USACEGSL
P PAPADOS
7701 TELEGRAPH RD
ALEXANDRIA VA 22315

1 AFOSR/NL
875 NORTH RANDOLPH ST
SUITE 325, RM 3112
F FAHROO
ARLINGTON VA 22203

5 SOUTHWEST RSRCH INST
C ANDERSON
K DANNEMANN
T HOLMQUIST
G JOHNSON
J WALKER
PO DRAWER 28510
SAN ANTONIO TX 78284

NO. OF
COPIES ORGANIZATION

1 COMPUTATIONAL MECH
CONSULTANTS
J A ZUKAS
PO BOX 11314
BALTIMORE MD 21239-0314

1 APPLIED RSCH ASSOCIATES
D E GRADY
4300 SAN MATEO BLVD NE
STE A220
ALBUQUERQUE NM 87110

1 INTERNATIONAL RSRCH
ASSOC INC
D L ORPHAL
4450 BLACK AVE
PLEASANTON CA 94566

3 ORNL
ENVIRONMENTAL SCI DIV
W DOLL
T GAMEY
L BEARD
PO BOX 2008
OAK RIDGE TN 37831

1 NATIONAL INST OF
STANDARDS & TECHLGY
BLDG & FIRE RSRCH LAB
J MAIN
100 BUREAU DR MS 8611
GAITHERSBURG MD 20899-8611

3 DIR USARL
RDRL D
V WEISS
RDRL SE
J PELLEGRINO
RDRL SES P
A EDELSTEIN
2800 POWDER MILL RD
ADELPHI MD 20783-1197

ABERDEEN PROVING GROUND

112 DIR USARL
RDRL D
M CHOWDHURY
RDRL WM
B FORCH
S KARNA
J MCCAULEY
P PLOSTINS
J SMITH

NO. OF
COPIES ORGANIZATION

RDRL WML
J NEWILL
M ZOLTOSKI
RDRL WML B
I BATYREV
B RICE
N WEINGARTEN
RDRL WML D
P CONROY
M NUSCA
RDRL WML G
M BERMAN
W DRYSDALE
RDRL WML H
T FARRAND
R SUMMERS
M FERREN-COKER
L MAGNESS
B SORESENSEN
E KENNEDY
T EHLERS
C MEYER
D SCHEFFLER
S SCHRAML
B SCHUSTER
RDRL WMM
R DOWDING
J ZABINSKI
RDRL WMM A
M MAHER
J TZENG
E WETZEL
RDRL WMM B
T BOGETTI
B CHEESEMAN
C FOUNTZOULAS
D HOPKINS
B POWERS
C RANDOW
M VANLANDINGHAM
R WILDMAN
C F YEN
RDRL WMM D
E CHIN
K CHO
R HOWELL
RDRL WMM E
M WILL-COLE
T JESSEN
J LASALVIA
J SANDS
RDRL WMM F
L KECSKES
S MATHAUDHU

NO. OF
COPIES ORGANIZATION

RDRL WMM G
J ANDZELM
A RAWLETT
RDRL WMP
P BAKER
S SCHOENFELD
RDRL WMP B
R BECKER
S BILYK
D CASEM
J CLAYTON
M GREENFIELD
C HOPPEL
R KRAFT
B LEAVY
B LOVE (10 CPS)
M SCHEIDLER
T WEERASOORIYA
C WILLIAMS (10 CPS)
RDRL WMP C
T BJERKE
S SEGLETES
G BOYCE
R MUDD
T DIGLIANI
N BRUCHEY
W WALTERS
RDRL WMP D
R DONEY
J RUNYEON
B SCOTT
D KLEPONIS
K STOFFEL
RDRL WMP E
M BURKINS
W GOOCH
T JONES
M LOVE
RDRL WMP F
R BITTING
E FIORAVANTE
A FRYDMAN
N GNIAZDOWSKI
R GUPTA
RDRL WMP G
N ELDREDGE
R EHLERS
W BUKOWSKI
B KRZEWINSKI
S KUKUCK
R BANTON
D KOOKER
G RANDERS-PEHRSON

INTENTIONALLY LEFT BLANK.